Optical characterization of Mg-doped GaN films grown by metalorganic chemical vapor phase deposition

G. Martínez-Criado,[a] A. Cros, and A. Cantarero
Materials Science Institute and Department of Applied Physics, University of Valencia, Dr. Moliner 50, 46100-Burjasot, Valencia, Spain

R. Dimitrov, O. Ambacher, and M. Stutzmann
Walter Schottky Institute, Technical University Munich, Am Coulombwall, 85748-Garching, Munich, Germany

(Received 3 February 2000; accepted for publication 29 June 2000)

Scanning electron microscopy, micro-Raman, and photoluminescence (PL) measurements are reported for Mg-doped GaN films grown on (0001) sapphire substrates by low-pressure metalorganic chemical vapor phase deposition. The surface morphology, structural, and optical properties of GaN samples with Mg concentrations ranging from 10^{19} to 10^{21} cm^{-3} have been studied. In the scanning micrographs large triangular pyramids are observed, probably due to stacking fault formation and three-dimensional growth. The density and size of these structures increase with the amount of magnesium incorporated in the samples. In the photoluminescence spectra, intense lines were found at 3.36 and 3.31 eV on the triangular regions, where the presence of cubic inclusions was confirmed by micro-Raman measurements. The excitation dependence and temperature behavior of these lines enable us to identify their excitonic nature. From our study we conclude that the interface region between these defects and the surrounding wurtzite GaN could be responsible for PL lines. © *2000 American Institute of Physics.* [S0021-8979(00)07719-7]

I. INTRODUCTION

The production of highly efficient blue and green light-emitting diodes[1] and the development of a violet injection laser[2] based on GaN have stimulated intensive research on this compound. Major advances have been achieved in the growth process of this material. A dual flow metalorganic chemical vapor deposition (MOCVD) growth process has been developed to promote two-dimensional GaN growth on sapphire.[3,4] The use of a low-temperature buffer layer has made possible the growth of device quality GaN films at high temperatures. For *p*-type doping of GaN by Mg, when MOCVD is used as the growth method, a postgrowth thermal treatment is necessary in order to convert the initially highly resistive Mg-doped GaN to lower resistance *p*-type GaN layers ($\sim 1\ \Omega\,cm$).[5,6]

Further progress towards advanced optoelectronic devices will require a better understanding of the defect formation and recombination processes in GaN epilayers. The lifetime of these optical devices is critically determined by defects such as dislocations, stacking faults, and inversion domain boundaries which can act as traps and recombination centers. Raman scattering and photoluminescence (PL) measurements have been employed as informative techniques for the structural and optical characterization of GaN films.[7–9] Raman spectroscopy is a very useful and straightforward tool for the quantitative determination of a minority phase in GaN.[10,11] The effect of doping, strain, and disorder can also be studied conveniently and with high sensitivity by this technique.[8] In addition, PL measurements provide information about the presence of impurities and their nature (shallow or deep centers).[12,13] Through the analysis of the luminescence spectrum as a function of various parameters important information on the nature of the electronic states can be obtained.

In this work we present the results of scanning electron microscopy (SEM), micro-Raman spectroscopy, and PL measurements on Mg-doped GaN samples with doping concentrations ranging from 10^{19} to 10^{21} cm^{-3}. The PL spectra were measured as a function of temperature, excitation energy, and excitation power in order to investigate the origin of the luminescence emissions found.

II. EXPERIMENTAL DETAILS

The Mg-doped GaN films analyzed here were grown on *c*-plane sapphire (α-Al_2O_3) substrates by low-pressure MOCVD. Bismethyl (cyclopentadienyl) magnesium (CP_2Mg) was employed as the *p*-type dopant precursor. To improve the structural properties of the films, first a 50 nm thick GaN nucleation layer was grown at 550 °C. After the growth of the low-temperature nucleation layer, the reactor temperature was raised to 950 °C to grow the Mg-doped GaN films. The GaN:Mg layers were between 0.5 and 1 μm thick. More details of the crystal growth have been described elsewhere.[7]

For the PL measurements the samples were mounted in a continuous He-flow cryostat. The temperature was varied from 5 to 300 K. For optical excitation three different ultraviolet lines of an Ar^+ laser were used (363.8 nm=3.41 eV, 351.2 nm=3.53 eV, and 333.6 nm=3.72 eV). The lumines-

[a]Permanent address: Department of General Physics, University of Havana, 10400-Vedado, Havana, Cuba; electronic mail: gmc@uv.es

cence light was detected with a 0.8 m DILOR double monochromator coupled to an ultraviolet-sensitive photomultiplier using photon counting techniques. The spectral resolution was 0.2 and 0.3 nm, and the integration time of the detector ranged from 5 to 10 s. The excitation power on the sample was typically 20–40 mW, with a spot diameter of ~ 500 μm.

The micro-Raman experiments were carried out at room temperature with a 0.8 m DILOR triple spectrometer equipped with a cooled charge-coupled device detector. The detailed setup for Raman-scattering measurements is described in Ref. 7. Raman spectra were taken in the backscattering geometry, with the laser beam along the *c* axis of the wurtzite structure [*z* direction, $(z(y,-)\overline{z})$]. The incident laser light was polarized along *x* or *y*, while the scattered light was collected with unspecified polarization (indicated with — in the above notation).

III. RESULTS AND DISCUSSION

A. Surface morphology

A HITACHI S-4100 scanning electron microscope with an electron beam energy of 15 keV was used to examine the surface of sample A([Mg]: 2×10^{19} cm^{-3}), as shown in Fig. 1(a). Small structures consisting of predominantly triangular and hexagonal shaped crystallites can be observed. The planar aspect of these structures is shown in detail in Fig. 2(a). In contrast, samples B ([Mg]: 4.5×10^{20} cm^{-3}) and C ([Mg]: 1×10^{21} cm^{-3}) exhibit large triangular pyramids, having a typical height of 4 μm and a width around 25 μm [Figs. 1(b) and 1(c), respectively]. Magnified views of two stages in the formation of these truncated pyramids are shown in Figs. 2(b) and 2(c). The pyramidal structure in Fig. 2(c) shows equally spaced steps, indicative of step bunching. The occurrence of such triangular structures suggest that the growth occurs faster along three well-defined preferential directions than along others. A similar growth behavior arises in the diamond lattice because of the particular arrangement of atoms and bonds.[14] As the magnesium content is increased by one order of magnitude, these equilateral triangular structures become somewhat thicker and more frequent, leading to a rougher appearance of the sample surface. This suggests that the presence of high magnesium concentrations catalyzes the formation of the triangular pyramids.

Similar surface morphologies have been observed in Si layers grown on (111) Si substrates by vapor deposition methods.[14,15] These investigations have proposed that the defects are formed by stacking faults through the following mechanism: faulted layers can result when (111) planes are incorrectly deposited. As the growth of the film proceeds, the defects spread laterally and grow mismatched with respect to the surrounding areas. The mismatched boundaries propagate from layer to layer along the three remaining (111) planes. Simultaneously, stair-rod dislocations along the [110] edges appear. The triangular form is most probable since it has the smallest edge length for atoms to attach to.[15] Mendelson has also studied the epitaxial growth of silicon for seven low-index orientations of the silicon substrates, showing that in all cases the shape of the mismatch boundary determines the geometrical form of the defect.[15] Among mechanically polished substrates, [111] substrates have the highest stacking fault density.

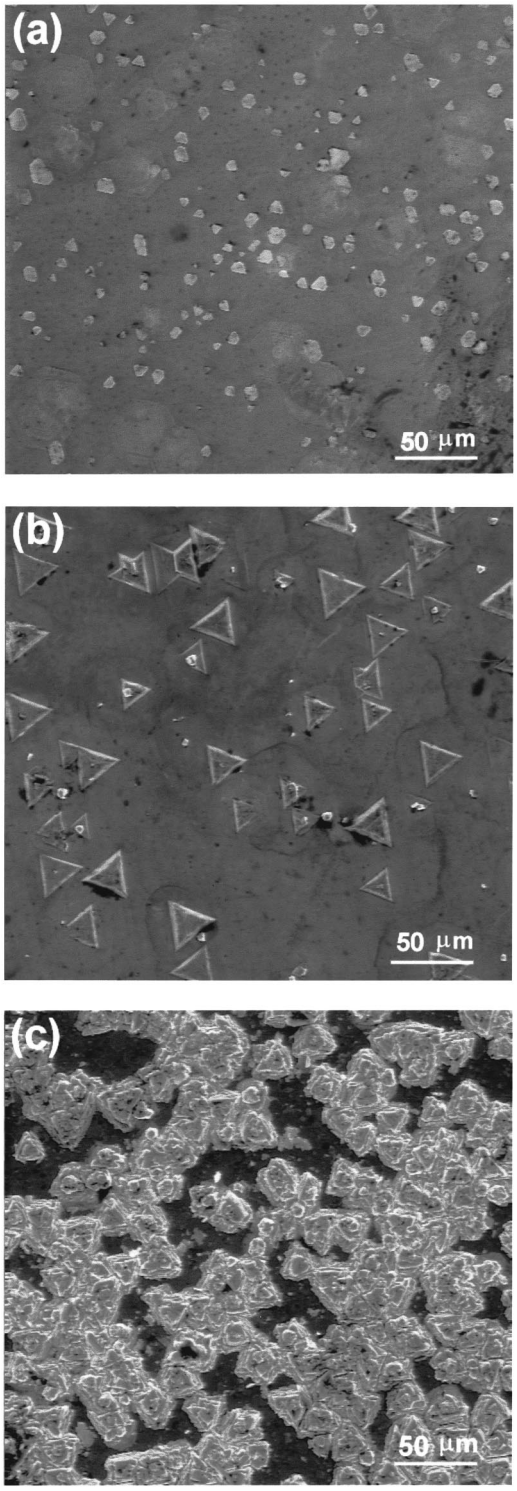

FIG. 1. Scanning electron micrographs of GaN samples with different concentration of magnesium: (a) [Mg]: 2×10^{19} cm^{-3}; (b) [Mg]: 4.5×10^{20} cm^{-3}; and (c) [Mg]: 10^{21} cm^{-3}. Marker indicates 50 μm.

The wurtzite and zincblende polytypes of GaN differ in their stacking sequences along the hexagonal *c* and cubic [111] axis: AaBbAaBb and AaBbCcAaBbCc for wurtzite and zincblende, respectively (capital letters

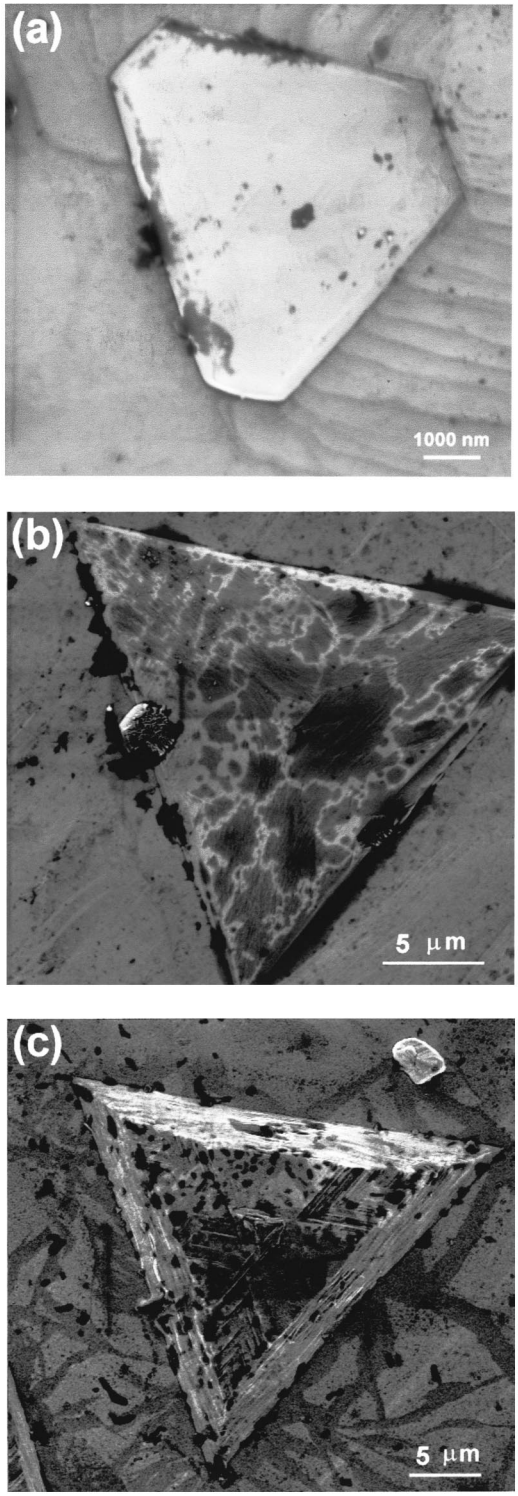

FIG. 2. Magnified views of the triangular defects found in the samples A and B: (a) planar feature of the triangular defect presents on the surface of the sample A; (b) and (c) show two stages of the truncated pyramid formation in the surface of the sample B.

correspond to Ga atoms and lowercase letters to N atoms). For wurtzite crystals, changes of this sequence, resulting from the removal or introduction of an extra layer, will produce AaBbAaBbCcBbCc (intrinsic type) or AaBbAaBbCcAcCcAa (extrinsic type) sequences, which contain units of an ideal zincblende structure (underlined).[16] Thus, taking into account the previous studies, the origin of the triangular structures could be explained if we assume that magnesium atoms occasionally initiate the formation of stacking faults on the hexagonal (0001) surface and transform the lattice into a cubic structure (i.e., $[111]_c \| [0001]_h$). In Fig. 2(a) a triangular defect on the surface of sample A, very similar to those found by Mendelson for silicon on a (111) substrate direction, can be clearly seen. The planar shape of this structure, also observable in sample B [Fig. 2(b)], suggests that the origin of these defects can be associated to stacking faults in the hexagonal matrix.

The occurrence of these defects is mainly controlled by the kinetics of the high quantity of magnesium impurities. It is well known that the presence of defects such as stacking faults, dislocations, and inversion domains enhances diffusion of impurities toward them.[17–19] Thus, additional magnesium atoms migrate towards these stacking faults causing them to grow laterally and tending to minimize the energy by island formation while preserving the triangular shape of the initial defect. Finally, the combined effect of stacking fault defects and three-dimensional growth results in triangular pyramids, whose density and sizes increase with the magnesium content on the surface. Energy-dispersive x-ray analysis indeed suggests a higher Mg concentration in the triangular structures compared to the surrounding material.

Similar surface defects in GaN nucleation layers grown on *c*-plane sapphire with a high density of stacking faults parallel to the film/substrate interface have been observed in other recent works.[20–22]

B. Optical characterization

In order to substantiate the importance of cubic stacking faults, we have performed micro-Raman measurements with the laser beam focused on the pyramid center and outside it. The spectra were taken in backscattering configuration, with the laser beam along the *c* axis of the wurtzite structure (*z* direction). As was already reported in Ref. 7, these triangular structures are characterized by the formation of cubic inclusions. In that previous work, transmission electron microscopy and micro-Raman measurements give evidence of the cubic GaN subdomain growth on the hexagonal matrix along the [0001] direction (i.e., [111] cubic direction) by the stacking fault mechanism. The Raman spectrum taken outside the triangular hillock exhibits the E_2 phonon mode at 568 cm^{-1} and the A_1 [longitudinal optical (LO)] mode at 735 cm^{-1}, characteristic of hexagonal, wurtzite GaN [Fig. 3(a)].

In addition, the spectrum from the pyramidal structure exhibits the cubic transverse optical (TO) mode at 555 cm^{-1} and the coupled LO phonon-plasmon mode at 512 cm^{-1}, typical of *n*-type samples. It is known that the formation of Mg–H complexes causes hole compensation.[23] Consequently, the presence of this latter mode indicates that the free electron concentration inside the triangular pyramid is higher than outside. Moreover, we found broad peaks at positions where local vibrational modes (LVM) and disorder activated Raman scattering in Mg-doped GaN films have been reported: 145, 269, 340, 364, 600, 660, 671, and 682 cm^{-1}.[24,25] The authors of Ref. 25 confirmed the previous

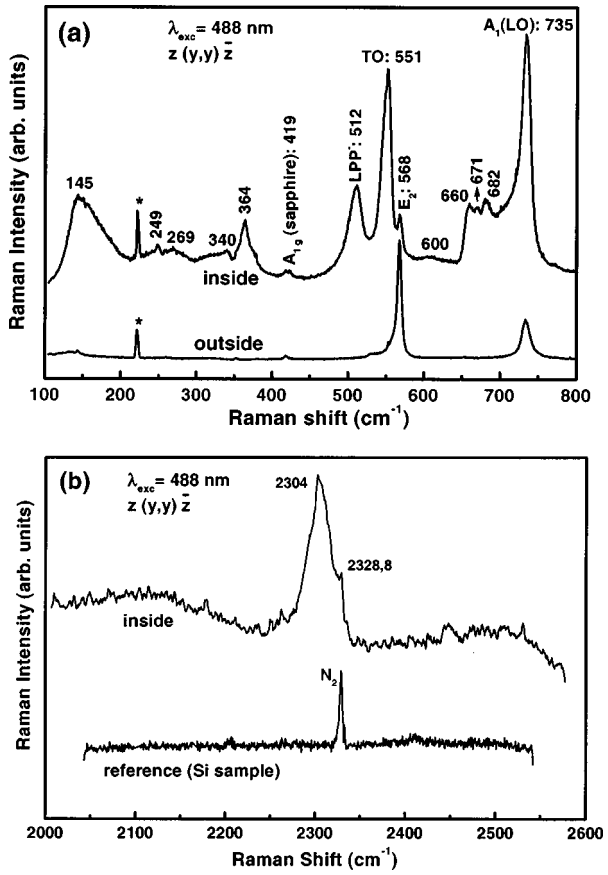

FIG. 3. Micro-Raman spectra taken with the laser beam focused on the pyramid center and outside it: (a) low-frequency region of the spectra; and (b) high-frequency region of the spectra. The assignment of the phonon modes is indicated in each spectrum. The plasma lines are labeled with asterisks in the figure.

assignments by calculations based on a modified valence-force model of Kane, obtaining frequencies of 132, 267, and 660 cm^{-1}. In the high energy region, unlike earlier work about LVM in Mg-doped GaN samples,[26,27] we found a peak at 2304 cm^{-1} but none around 2200 cm^{-1} [Fig. 3(b)]. The line N_2 vibrations in air was also observed at 2328.8 cm^{-1} in our spectra.

Figure 4(a) shows low temperature PL spectrum measured in the region with the highest density of triangles in sample A. In contrast, spectrum 4(b) was taken on a defect-free region (i.e., region without triangular structures). No free and shallow-bound exciton emissions of the hexagonal GaN or cubic GaN are observed in the spectra, indicating the presence in both regions of additional nonradiative recombination channels typical for a relatively high Mg-doping level. For instance, the acceptor–H neutral complexes found in Mg doped GaN films, cause deep-level and blue emissions in the PL spectra besides the hole compensation.[23] The local fields produced by such defects, as well as fluctuations of the location of the atoms in the crystal, induce the exciton dissociation, making the excitonic transitions undetectable. Instead, we see a complex structure of strong lines related to the triangular pyramids [Fig. 4(a)], accompanied by the ''yellow band'' emission around 2.38 eV. In the defect-free region, the luminescence is completely dominated by a broad

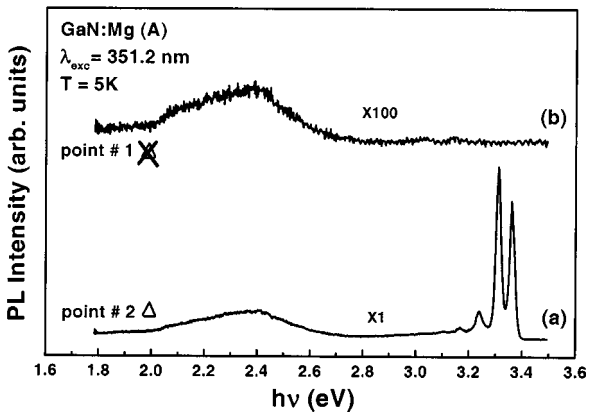

FIG. 4. Photoluminescence spectra on different surface regions at 5 K in the sample A: (a) spectrum measured on a high polygonal crystallites density region; and (b) spectrum taken on a defect-free region.

band centered 2.35 eV, with a full width at half maximum of 300 meV [Fig. 4(b)]. It is important to note that from our PL measurements on the substrates, we do not find any luminescence from sapphire. The PL results show a variable distribution of the radiative centers in the sample, in accordance with the surface morphology and structural properties observed by SEM and micro-Raman measurements.

The PL spectra for three samples with different Mg content are shown in Fig. 5, taken with the laser beam focused on regions of a high density of triangles. Unexpectedly, the

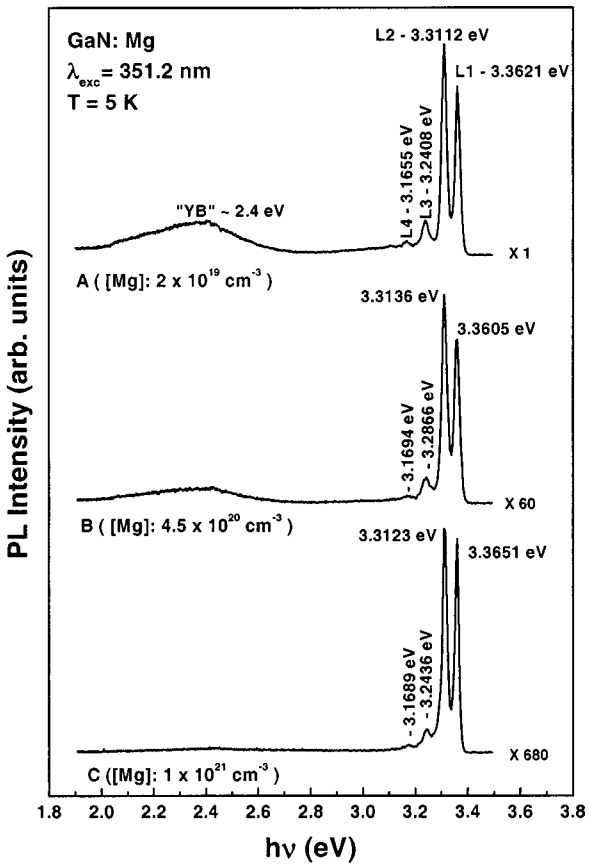

FIG. 5. Photoluminescence spectra at 5 K of GaN samples with different concentration of magnesium.

spectra do not show a significant variation from sample to sample, in spite of the notable changes in the surface morphology and the magnesium content; previously reported Mg-related transitions are not observed either.[28,29] Unlike typical GaN PL spectra, the luminescence here is clearly dominated by two lines at 3.36 (L1) and 3.31 eV (L2), significantly below the hexagonal GaN band gap ($E_g = 3.50$ eV),[30] and slightly above the cubic GaN band gap ($E_g = 3.30$ eV).[31] Their narrow linewidths of 10 and 14 meV, respectively, suggest an excitonic nature. Identical peaks have been observed in layers grown by different techniques, with dissimilar dopants and on different substrates. These emission lines have been assigned either to deeply bound excitons in structurally distributed regions,[32,33] to near-band gap emissions in cubic GaN,[34] or dislocation bound excitons.[35] Some works have tentatively attributed these transitions to phonon replicas of shallow-bound excitons or localized defect levels, such as nitrogen vacancies.[32,36–38] Incorporation of cubic phase in wurtzite material has been reported as well.[9] The notably invariant energetic position of these lines, also independent of the magnesium concentration in our samples, suggests a connection with localized centers associated to imperfections in the intrinsic GaN structure, such as stacking faults. In addition, there are two weak transitions below L2 at 3.25 eV (L3) and 3.17 eV (L4), whose nature will be discussed later.

As can be observed from Fig. 5, the ''yellow band'' (YB) is a competitive radiative recombination channel with respect to the former transitions in the three samples. Many of the GaN samples exhibit this broad Gaussian-shaped band centered between 2.2 and 2.4 eV.[39–41] Native defects (vacancies, interstitials), dislocations, and residual impurities (such as carbon[42]) represent intrinsic candidates for the origin of this band but its nature is still unclear. Two models have been suggested to explain the recombination mechanism of the YB: (i) Ogino and Aoki[43] proposed that the initial state is a shallow donor and the final state is a deep acceptor (about 0.86 eV above the valence band), and (ii) Glaser *et al.*[44] concluded that this transition involves a deep donor (with a level depth of about 1.0 eV) and, therefore, a shallow acceptor about 0.2 eV above the valence band. The nature of the deep level has not been determined; it has been argued that it has an intrinsic origin, such as nitrogen antisites.[45] Moreover, Zhang *et al.*[46] varied the MOCVD growth conditions to correlate a contribution of gallium vacancies to the formation of this localized gap state.

In general, a decrease in the overall luminescence intensity with the magnesium doping is clearly visible from our spectra, possibly due to diffusion of both laser beam and PL emission on the rough surfaces. Furthermore, a relative decrease of the YB can be appreciated, showing the samples with higher magnesium content a smaller intensity of this band. This behavior is coherent with a deep level associated with Ga vacancies, as mentioned before, which might disappear when magnesium enters on Ga sites for higher concentrations in the layer.[46]

In view of the partial overlapping of the spectral lines in our PL spectra, we carried out its decomposition using a multi-Gaussian fitting procedure. This analysis suggests the presence of two small additional peaks: at the high energy side of the L1 line (X1), and at the low energy side of the L2 emission (X2) for sample C, as shown in Fig. 6. The existence of the additional peak X1 becomes more evident from the analysis of the luminescence thermal dependence, which will be discussed later. The identification of these transitions will be pursued in the following subsections, based on the evolution of the PL spectra with the excitation photon energy, excitation power, and temperature.

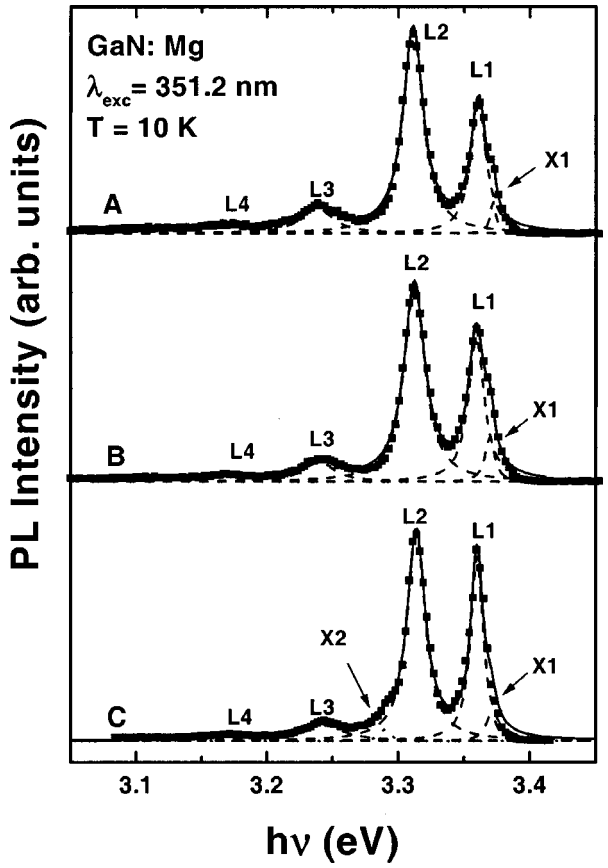

FIG. 6. Photoluminescence spectra of the three sample and the multi-Gaussian fitting.

1. Excitation photon energy dependence

Typical PL spectra for three different excitation wavelengths (333.6, 351.2, and 363.8 nm) are shown in Fig. 7 for sample A. The L1 and L2 emissions dominate the PL spectra, both when exciting below and above the hexagonal GaN band gap, suggesting that these lines are independent of the hexagonal interband transitions. Simultaneously, as there are no other peaks at higher energies, the interpretation of L1 and L2 as phonon replicas of higher energy transitions can be ruled out.

It can also be seen from Fig. 7 that the relative intensity of the L1 line (3.36 eV) decreases with the excitation photon energy, becoming this decay more appreciable for $\lambda_{exc} = 363.8$ nm (3.41 eV). Such a behavior indicates a lower population of the higher energy states, which may be caused by two combined effects: a nonuniform distribution of the pumped carrier energy, and the discrete character of relaxation processes by optical phonons.

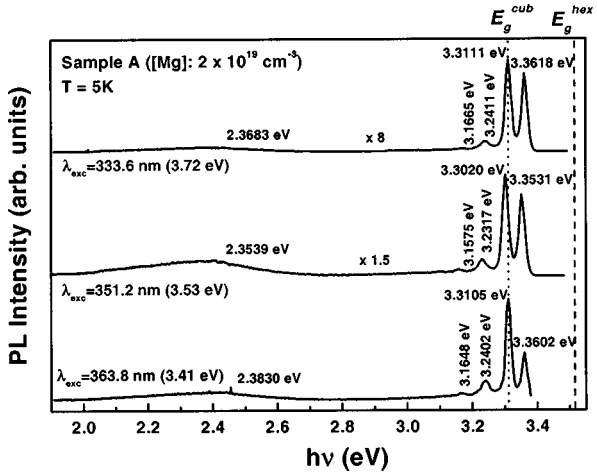

FIG. 7. Photoluminescence spectra of the sample A for three different excitation wavelengths.

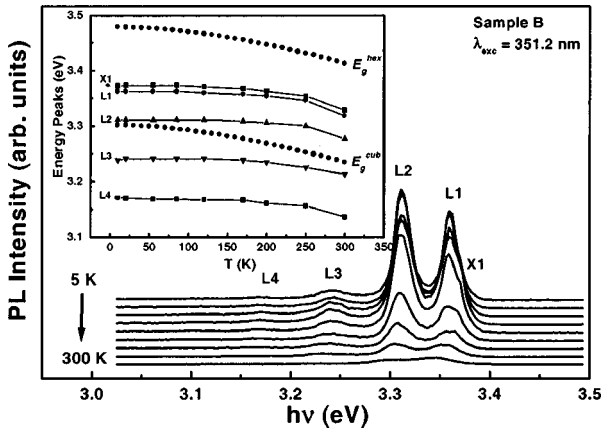

FIG. 9. Photoluminescence spectra as a function of temperature for sample B. The inset shows the peak positions of the different spectral lines as a function of temperature. The empirical dependencies of the hexagonal and cubic GaN energy gap are included in the figure for comparison.

2. Excitation power dependence

To provide further information on the origin of these PL lines, we recorded the PL spectra for various excitation intensities, spanning a dynamic range of two decades. Typical spectra are shown in Fig. 8 for sample A. The L1 and L2 lines have the common feature of showing no shift with intensity, consistent with a bound exciton emission origin.[34,47] On the other hand, their linewidths increase for high excitation density, with a little increasing asymmetry towards higher energies, perhaps suggesting a donor–acceptor pair origin. However, we must be cautious about this identification.

In the inset of Fig. 8 the integrated intensities for the two high energy peaks L1 and L2 (obtained from Gaussian fits to the line shapes) are plotted as a function of the excitation power for sample A. As can be seen from this graph, the intensity increases about 100 times when the excitation power is increased by the same factor. By using a power law dependence of luminescence intensity I on the excitation power P, $I \propto P^n$, a value of $n = 1.15$ is obtained from the fitting. This behavior accentuates the evidence for the excitonic nature of these lines instead of a donor–acceptor pair recombination character.

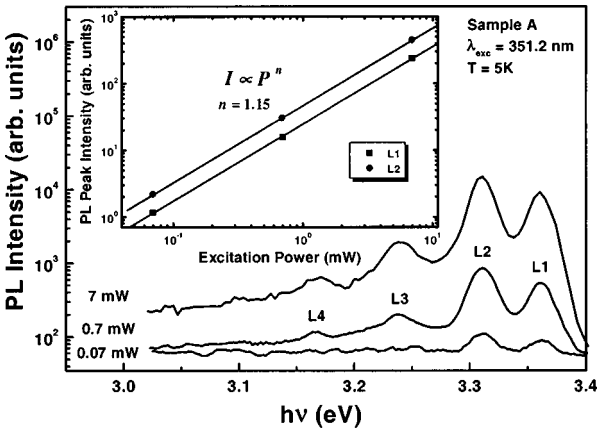

FIG. 8. Variation of the photoluminescence spectra with excitation power for the sample A at 5 K. The inset shows the excitation power dependence of the integrated intensity of the L1 and L2 emissions. Solid lines show fits to power-law variation with the same exponent $n = 1.15$ for the two lines.

3. Temperature dependence

Figure 9 shows the PL spectra in the 10–300 K range measured from sample B. The PL intensity slightly increases for a sample temperature up to about 80 K. Above this value, we can observe a luminescence quenching, but the emission lines can even be easily observed up to 300 K. In general, they broaden and shift to lower energies as the temperature rises. For the spectra recorded above 200 K the intensity of the L1 peak diminishes, and the small thermally-activated X1 peak becomes more evident. The PL evolution is very similar for samples A and C, although the latter shows a markedly faster quenching for temperatures above 80 K, becoming the signal almost undetectable for temperatures higher than 170 K.

The energies of the different peaks in the spectra are plotted as a function of the temperature in the inset of Fig. 9. A small monotonic shift to lower energies can be seen with the increase in temperature. The empirical dependencies of the hexagonal and cubic GaN energy gaps are included in the figure for comparison.[31,48] Since no well-defined blueshift of the main emissions (X1, L1, and L2) was observed with increasing temperature, the possibility of a donor–acceptor pair recombination is discarded.[46] On the other hand, as the temperature has been raised, the dominant shift in the L3 and L4 peak positions is in close agreement with that of the L1 emission. Based on the energy distances among these lines and on the micro-Raman measurements, these two low energy bands have been assigned to phonon-assisted replicas of the 3.310 eV (L2) recombination line corresponding to the emission of one and two TO phonons (70 meV), respectively.

An analysis of their thermal dependencies gives a mean energy shift in the X1, L1, and L2 lines of about 40 meV for the 10–300 K range, which is smaller than the band gap shrinkage of bulk *h*-GaN and *c*-GaN ($\Delta E_g^{hex} \approx \Delta E_g^{cub} \approx 66$ meV). This discrepancy can be explained if we assume that

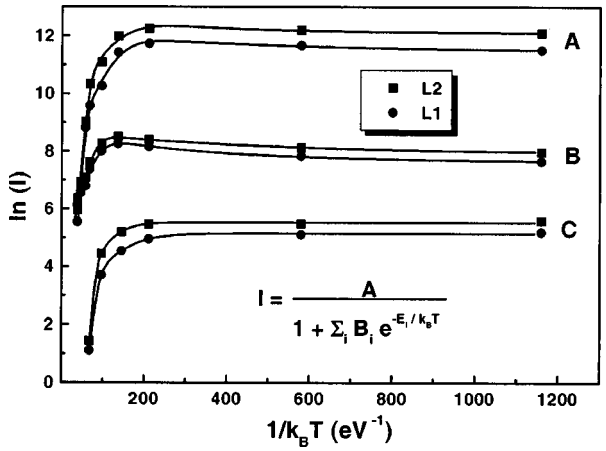

FIG. 10. Arrhenius plots of the integrated intensity of L1 and L2 emissions vs $1/k_BT$ for the three samples. Solid curves represent theoretical fits to Eq. (1).

our peaks L1 and L2 are the integral overlapping of several energy states, partially resolved in the multi-Gaussian fit of Fig. 6, and totally resolved by Hong *et al.*[34] When the temperature increases, the higher levels of this complex become filled, shifting the peak against the typical band gap shrinkage effect. These excitonic lines could be associated to different types of stacking faults or some complex defects involving them. Bandić *et al.*[49] investigated stacking faults in GaN using local empirical pseudopotentials and identified an interface state within the band gap about 0.13 eV above the valence band maximum. On the other hand, Stampfl and Van de Walle[50] found no defect-induced localized states in the band gap from first-principles calculations. Their investigation showed that the zincblende/wurtzite interface exhibits a type-II lineup with $\Delta E_v \approx 0.07$ eV and $\Delta E_c \approx 0.27$ eV, supporting the suggestion that the stacking faults can give rise to quantum-well-like regions of zincblende material embedded in the wurtzite matrix that can bind excitons. However, we exclude this possibility as the origin of our PL lines because identical luminescence features have been found in high purity cubic GaN samples (with a volume fraction of hexagonal subdomains smaller than 1%).[10] Alternatively, we believe that the interface region between these defects could be responsible for these bound exciton lines. They may be understood as result of the electron–hole recombinations at regions where the binding potential is uniformly distributed over several lattice sites, i.e., defects which exhibit small changes in their local environment between nearly equivalent sites. This is to be contrasted with binding, essentially, at a single site as in a shallow-bound exciton, where either the electron or the hole is weakly bound in a central force potential.

Figure 10 shows the natural logarithm of the integrated intensity of L1 and L2 versus $1/k_BT$ for the three samples. In general, two different temperature regions can be distinguished: at low temperatures, up to 80 K, we detect a slight increase while above this value a very rapid quenching is observed. An analysis of these data has been carried out using the well known thermal activation relation[51]

$$I = \frac{A}{1 + \Sigma_i B_i e^{-E_i/k_B T}}. \tag{1}$$

Detailed evaluation shows that two activation energies are sufficient for a satisfactory fit of B and C results, whereas a third mechanism is necessary for fitting L1 and L2 intensities in sample A. The respective activation energies obtained from the fitting procedure for the three samples are given in the columns E_1, E_2, and E_3 of Table I. The energy difference $\Delta E = E_g^{\text{hex}} - h\nu$ ($h\nu$: energy of the L1 and L2 transitions), and the binding energy E_B of the excitons to the attractive centers at 10 K ($E_B = \Delta E - E_X$; $E_X = 26$ meV: free exciton energy) are also listed in the table.

Beginning from 10 K in samples A and B, a first exciton capture process dominates with very low activation energy E_1, due to the slight increase of the PL intensity for this temperature range (10–55) K. We shall now identify the dissociation process leading to the activation energies E_2 and E_3. There are four different processes for the dissociation of the defect bound exciton lines: (d_{L1}^0, X) and (d_{L2}^0, X). From these possibilities different dissociation energies ($E_{a,b}$) result, which will be compared with the determined energies E_2 and E_3. Four different dissociation mechanisms have been considered:

(a) dissociation resulting in a free exciton

$$(d_{Li}^0, X) \rightarrow d_{Li}^0 + X,\ E_a = E_B; \tag{2}$$

(b) dissociation resulting in one free electron and one free hole

TABLE I. Activation energies are shown for the two fundamental transitions (L1 and L2) obtained from the theoretical fits of the temperature dependence of intensity to Eq. (1) for the three GaN:Mg samples. The transition energies of these emissions ($h\nu$) and the binding energies deduced from them (E_B) at 10 K are also listed.

Sample	Peak	$h\nu$ (eV)	$E_g^{\text{hex}} - h\nu$ (meV)	E_B (meV)	E_1 (meV)	E_2 (meV)	E_3 (meV)	B_1	B_2	B_3	A
A	L1	3.3617	138.3	112.3	1.9	31.6	200	−0.509	4529	9.6×10^6	11.46
	L2	3.3112	188.8	162.8	3.5	23.1	161	−0.614	15.45	2×10^6	12.10
B	L1	3.3608	139.2	113.2	2.3	48.3	⋯	−0.70	26.02	⋯	7.62
	L2	3.3122	187.8	161.8	1.6	65.5	⋯	−0.557	73.78	⋯	7.89
C	L1	3.3605	139.5	113.5	⋯	20	138	⋯	15.64	6.2×10^6	5.14
	L2	3.3137	183.6	160.3	⋯	32	190	⋯	30.87	2.4×10^8	5.52

$$(d^0_{Li},X)\rightarrow d^0_{Li}+e+h,\ E_b=E_B+E_X; \quad (3)$$

(c) dissociation resulting in one free hole and two free electrons

$$(d^0_{Li},X)\rightarrow d^+_{Li}+h+e+e,\ E_c=E_B+E_X+E_{\text{dioniz}}\gg E_b; \quad (4)$$

(d) dissociation resulting in one free electron

$$(d^0_{Li},X)\rightarrow(d^+_{Li},X)+e,\ E_d=E_B+E_X-E(d^0_{Li})<E_b. \quad (5)$$

It is evident that only the dissociation of a free electron from the complex can cause the first intensity drop (E_2). The activation energies of the other processes are too high to explain the results. This means that the binding energy of the second electron in the complex is lower than the ionization energy of the free exciton. Thus, the neutral center is repulsive to a second electron, and the binding must be mediated by the hole.

Finally, at higher temperatures the intensity decreases more rapidly and another dissociation process begins to dominate with an activation energy E_3. We can observe that the energies E_3 and E_B+E_X which are listed in Table I are approximately equal to each other. Therefore, we can describe this process by the dissociation resulting in one free electron and one free hole [process (b)]. All other possible cases cannot be brought into agreement with the data.

IV. CONCLUSIONS

We have investigated Mg-doped GaN films with Mg concentration ranging from 10^{19} to 10^{21} cm^{-3} by means of scanning electron microscopy, micro-Raman, and photoluminescence measurements. The scanning micrographs show triangular pyramids, probably due to stacking faults formation and three-dimensional growth controlled by the kinetic of the high quantity of Mg impurities. The magnesium local vibrational modes, observed in the micro-Raman spectra taken inside the pyramidal structures, indicate higher Mg incorporation in these defects. On the other hand, intense lines were found at 3.36 and 3.31 eV in the photoluminescence spectra from the triangular regions. Their excitation dependencies and temperature behavior enable us to identify them as excitonic complexes. From our study we concluded that the interface region between these defects could be responsible for these PL lines. Finally, the dissociation of the excitonic complexes was investigated from the thermal dependence of the integrated intensity. All samples show qualitatively the same behavior. First, the dissociation of electrons from the excitonic complexes reduces the emissions, whereas for increasing temperature both holes and electrons contribute to the thermal quenching.

ACKNOWLEDGMENTS

The authors thank A. Homs-Purón for his useful discussions and comments. One author (G.M.-C.) acknowledges the Walter Schottky Institute and the Generalitat Valenciana for financial support.

[1] S. Nakamura, M. Senoh, S. Nagahama, N. Iwasa, Y. Yamaha, T. Matsuchita, H. Kiyoku, and Y. Sugimoto, Jpn. J. Appl. Phys., Part 2 **53**, L74 (1996).
[2] S. Nakamura, M. Senoh, S. Nagahama, N. Iwasa, Y. Yamaha, T. Matsushita, Y. Sugimoto, and N. Kiyoku, Appl. Phys. Lett. **70**, 1417 (1997).
[3] H. Amano, N. Sawaki, I. Akasaki, and Y. Toyoda, Appl. Phys. Lett. **48**, 353 (1986).
[4] S. Nakamura, Jpn. J. Appl. Phys., Part 2 **30**, L1705 (1991).
[5] S. Nakamura, T. Mukai, M. Senoh, and N. Iwasa, Jpn. J. Appl. Phys., Part 2 **31**, L139 (1992).
[6] H. Amano, M. Kito, K. Hiramatsu, and I. Akasaki, Jpn. J. Appl. Phys., Part 2 **28**, L2112 (1989).
[7] A. Cros, R. Dimitrov, H. Angerer, O. Ambacher, M. Stutzmann, S. Christiansen, M. Albrecht, and H. P. Strunk, J. Cryst. Growth **181**, 197 (1997).
[8] W. Rieger, T. Metzger, H. Angerer, R. Dimitrov, O. Ambacher, and M. Stutzmann, Appl. Phys. Lett. **68**, 970 (1996).
[9] W. Rieger, R. Dimitrov, D. Brunner, E. Rohrer, O. Ambacher, and M. Stutzmann, Phys. Rev. B **54**, 17 596 (1996).
[10] H. Siegle, L. Eckey, A. Hoffmann, C. Thomsen, and B. K. Meyer, Solid State Commun. **96**, 943 (1995).
[11] M. Giehler, M. Ramsteiner, O. Brandt, H. Yang, and K. H. Ploog, Appl. Phys. Lett. **67**, 733 (1995).
[12] K. K. Sheu, Y.K. Su, G. C. Chi, B. J. Pong, C. Y. Chen, C. N. Huang, and W. C. Chen, J. Appl. Phys. **84**, 4590 (1998).
[13] E. Oh, H. Park, and Y. Park, Appl. Phys. Lett. **72**, 70 (1998).
[14] G. R. Booker and R. Stickler, J. Appl. Phys. **33**, 3281 (1962).
[15] S. Mendelson, J. Appl. Phys. **65**, 1570 (1964).
[16] N. E. Christensen and P. Perlin, in *Gallium Nitride I*, Semiconductors and Semimetals Series, Vol. 50, edited by J. I. Pankove and T. D. Moustakas (Academic, New York, 1998).
[17] Q. Zhu, A. Botchkarev, W. Kim, O. Aktas, A. Salvador, B. Sverdlov, H. Morkoç, S.-C.-Y. Tsen, and D. J. Smith, Appl. Phys. Lett. **68**, 1141 (1996).
[18] Z. Liliental-Weber *et al.*, Mater. Res. Soc. Symp. Proc. **423**, 487 (1996).
[19] G. Popovici, W. Kim, A. Botchkarev, H. Tang, H. Morkoç, and J. Solomon, Appl. Phys. Lett. **71**, 3385 (1997).
[20] X. H. Wu, D. Kalponek, E. J. Tarsa, B. Heying, S. Keller, B. P. Keller, U. K. Mishra, S. P. DenBaars, and J. S. Speck, Appl. Phys. Lett. **68**, 1371 (1996).
[21] X. H. Wu, P. Fini, S. Keller, E. J. Tarsa, B. Heying, U. K. Mishra, S. P. DenBaars, and J. S. Speck, Jpn. J. Appl. Phys., Part 2 **35**, L1648 (1996).
[22] L. Cheng, G. Zhang, D. Yu, and Z. Zhang, Appl. Phys. Lett. **70**, 1408 (1997).
[23] S. Nakamura, N. Iwasa, M. Senoh, and T. Mukai, Jpn. J. Appl. Phys., Part 1 **31**, 1258 (1992).
[24] H. Harima, T. Inoue, S. Nakashima, M. Ishida, and M. Taneya, Appl. Phys. Lett. **75**, 1383 (1999).
[25] A. Kaschner, H. Siegle, G. Kaczmarczyk, M. Strassburg, A. Hofmann, C. Thomsen, U. Birkle, S. Einfeldt, and D. Hommel, Appl. Phys. Lett. **74**, 3281 (1999).
[26] W. Götz, N. M. Johnson, D. P. Bour, M. D. McCluskey, and E. E. Haller, Appl. Phys. Lett. **69**, 3725 (1996).
[27] M. S. Brandt, W. W. Ager III, W. Götz, N. M. Johnson, J. S. Harris, R. J. Molnar, and T. D. Moustakas, Phys. Rev. B **49**, R14 758 (1994).
[28] T. W. Kang, S. H. Park, H. Song, T. W. Kim, G. S. Yoon, and C. O. Kim, J. Appl. Phys. **84**, 2082 (1998).
[29] A. K. Viswanath, E.-J. Shin, J. I. Lee, S. Yu, D. Kim, B. Kim, Y. Choi, and C.-H. Hong, J. Appl. Phys. **83**, 2272 (1998).
[30] D. Volm *et al.*, Phys. Rev. B **53**, 16 543 (1996).
[31] G. Ramírez-Flores, H. Navarro-Contreras, A. Lastras-Martínez, R. C. Powell, and J. E. Greene, Phys. Rev. B **50**, 8433 (1994).
[32] C. Wetzel, S. Fischer, J. Krüger, E. E. Haller, R. J. Molnar, T. D. Moustakas, E. N. Mokhov, and P. G. Baranov, Appl. Phys. Lett. **68**, 2556 (1996).
[33] M. Cazzanelli, D. Cole, J. F. Donegan, J. G. Lunney, P. G. Middleton, K. P. O'Donnell, C. Vinegoni, and L. Pavesi, Appl. Phys. Lett. **73**, 3390 (1998).
[34] C. H. Hong, D. Paulidis, S. W. Brown, and S. C. Rand, J. Appl. Phys. **77**, 1705 (1995).
[35] P. Thurian *et al.*, in *Proceedings of International Symposium on Blue Laser and Blue Light Emitting Diodes*, edited by A. Yoshikawa, K. Kishino, M. Kobayashi, and T. Yasuda (Institute of Physics, 1996), p. 180.
[36] R. Dingle, D. D. Sell, S. E. Stokowski, and M. Ilgems, Phys. Rev. B **4**, 1211 (1971).
[37] R. Dai, S. Fu, J. Xie, G. Fan, G. Hu, H. Schrey, and C. Klingshirn, J. Phys. C **15**, 393 (1982).

[38] O. Lagerstedt and B. Monemar, J. Appl. Phys. **45**, 2266 (1974).
[39] H. M. Chen, Y. F. Chen, M. C. Lee, and M. S. Feng, Phys. Rev. B **56**, 6942 (1997).
[40] R. H. Molnar and T. D. Moustakas, J. Appl. Phys. **76**, 4587 (1997).
[41] C. Wetzel, D. Volm, B. K. Meyer, K. Pressel, S. Nilsson, E. N. Mokhov, and P. G. Baranov, Appl. Phys. Lett. **65**, 1033 (1994).
[42] R. Zhang and T. F. Kuech, Appl. Phys. Lett. **72**, 1611 (1998).
[43] T. Ogino and M. Aoki, Jpn. J. Appl. Phys. **19**, 2395 (1980).
[44] E. R. Glaser, T. A. Kennedy, K. Doverspike, L. B. Rowland, D. K. Gaskill, J. A. Freitas, Jr., M. Asif Khan, D. T. Olson, J. K. Kuznia, and D. K. Wickenden, Phys. Rev. B **51**, 13 326 (1995).
[45] T. Suski, P. Perlin, H. Teisseyre, M. Leszczynski, I. Grzegory, J. Jun, M. Bockowsji, S. Porowski, and T. Moustakas, Appl. Phys. Lett. **67**, 2188 (1995).
[46] X. Zhang, P. Kung, D. Walker, A. Saxler, and M. Razeghi, Mater. Res. Soc. Symp. Proc. **395**, 625 (1996).
[47] K. Naniwae, S. Itoh, H. Amano, K. Itoh, K. Hiramatsu, and I. Akasaki, J. Cryst. Growth **99**, 381 (1990).
[48] E. Calleja and R. Beresford, Semicond. Sci. Technol. **12**, 1396 (1997).
[49] Z. Z. Bandic, T. C. McGill, and Z. Ikonić, Phys. Rev. B **56**, 3564 (1997).
[50] C. Stampfl and Chris G. Van de Walle, Phys. Rev. B **57**, R15 052 (1998).
[51] D. Bimberg, M. Sondergeld, and E. Grobe, Phys. Rev. B **4**, 3451 (1971).